Modified mean-field theory of the magnetic properties of concentrated, high-susceptibility, polydisperse ferrofluids

Anna Yu. Solovyova, Ekaterina A. Elfimova, and Alexey O. Ivanov
Department of Theoretical and Mathematical Physics, Institute of Natural Sciences and Mathematics, Ural Federal University, 51 Lenin Avenue, Ekaterinburg 620000, Russia

Philip J. Camp*
School of Chemistry, University of Edinburgh, David Brewster Road, Edinburgh EH9 3FJ, Scotland and Department of Theoretical and Mathematical Physics, Institute of Natural Sciences and Mathematics, Ural Federal University, 51 Lenin Avenue, Ekaterinburg 620000, Russia
(Received 6 September 2017; published 27 November 2017)

The effects of particle-size polydispersity on the magnetostatic properties of concentrated ferrofluids are studied using theory and computer simulation. The second-order modified mean-field (MMF2) theory of Ivanov and Kuznetsova [Phys. Rev. E **64**, 041405 (2001)] has been extended by calculating additional terms of higher order in the dipolar coupling constant in the expansions of the initial magnetic susceptibility and the magnetization curve. The theoretical predictions have been tested rigorously against results from Monte Carlo simulations of model monodisperse, bidisperse, and highly polydisperse ferrofluids. Comparisons have been made between systems with the same Langevin susceptibility and the same saturation magnetization. In all cases, the new theoretical magnetization curve shows better agreement with simulation data than does the MMF2 theory. As for the initial susceptibility, MMF2 theory is most accurate for the monodisperse model, while the new theory works best for polydisperse systems with a significant proportion of large particles. These results are important for the analysis and characterization of recently synthesized polydisperse ferrofluids with record-breaking values of the initial magnetic susceptibility.

DOI: 10.1103/PhysRevE.96.052609

I. INTRODUCTION

Ferrofluids consist of ferromagnetic or ferrimagnetic nanoparticles suspended in magnetically passive carrier liquids. These systems can be classified as highly functional materials due to the unique combination of physical, electromagnetic, and optical properties, which can be controlled by applied magnetic fields or magnetic field gradients [1]. The diameters of the magnetic cores are typically in the region of 10 nm, which for commonly used materials such as magnetite (Fe_3O_4) means that each particle contains a single magnetic domain, and hence the ferrofluid can be described as a superparamagnetic material. The granulometric composition is rarely uniform within a given sample of ferrofluid, and therefore one needs to consider particle-size polydispersity. An effective way to determine the particle-size distribution within a sample is to analyze theoretically the magnetic properties, such as the magnetization curve and the initial susceptibility. Alternative methods such as counting particles in microscopy images are tedious and subject to considerable sampling errors.

The constituent particles in a ferrofluid are usually modeled as dipolar hard spheres with a magnetic core diameter x and a nonmagnetic layer of thickness $\delta \simeq 2$ nm representing the "dead" layer at the surface of a particle and the thickness of an adsorbed layer of sterically stabilizing surfactant molecules; the effective hard-sphere diameter is therefore $\sigma = x + 2\delta$. The magnetic moment on a particle is estimated from the bulk saturation magnetization M_s to be $\mu = \pi x^3 M_s/6$. Many theoretical methods have been developed to study the magnetization curve and initial susceptibility of monodisperse and polydisperse ferrofluids. The oldest and simplest theoretical approach is the Langevin single-particle model of an ideal superparamagnetic gas of noninteracting particles [2] according to which the magnetization curve and initial susceptibility are given, respectively, by [3]

$$M_L(H) = \rho\left\langle \mu(x) L\left(\frac{\mu_0 \mu(x) H}{k_B T}\right)\right\rangle \tag{1}$$

$$\chi_L = \left(\frac{\partial M_L}{\partial H}\right)_{H=0} = \frac{\mu_0 \rho \langle \mu^2(x)\rangle}{3 k_B T}, \tag{2}$$

where H is the external magnetic field, $\rho = N/V$ is the number concentration of particles in a volume V, k_B is Boltzmann's constant, T is the temperature, μ_0 is the vacuum permeability, $L(z) = \coth z - z^{-1}$ is the Langevin function, and the angular brackets denote an average over the particle-size distribution $p(x)$:

$$\langle f(x)\rangle = \int_0^\infty p(x) f(x) dx. \tag{3}$$

Apart from the number concentration ρ, there is the hard-sphere volume fraction

$$\varphi = \frac{\pi \rho \langle \sigma^3(x)\rangle}{6}, \tag{4}$$

which is typically of order 0.1 in standard ferrofluids. One can also define a magnetic volume fraction

$$\varphi_m = \frac{\pi \rho \langle x^3\rangle}{6} = \frac{M(\infty)}{M_s}. \tag{5}$$

*Author to whom all correspondence should be addressed: philip.camp@ed.ac.uk

 ©2017 American Physical Society

In practice, experimental measurements of χ show that it increases more rapidly with concentration than is predicted by the linear Langevin law (2) [4]. This is due primarily to the dipole-dipole interactions between the particles. One physically intuitive method of including such interactions is to use the Langevin expressions but with an effective magnetic field $H_{\rm eff} = H + \frac{1}{3}M(H)$ including the magnetization of the fluid, leading to a transcendental equation for the magnetization curve [5,6], and the prediction of spontaneous magnetization at low temperature and/or high concentration, which has never been observed in experiments. Other methods are based on quite general liquid-state approaches, such as integral equations with the mean-spherical approximation closure [7–9], thermodynamic perturbation theory [10–12], so-called modified mean-field (MMF) theories [13,14], formal Mayer-type cluster expansions [15,16], and density-functional theory [17–19]. All of these approaches work quite well for ferrofluids with low-to-moderate content of magnetic material and where dipole-dipole interactions are not very strong. In Refs. [20,21], all of the then-available theories were tested critically by determining the polydispersity from experimental measurements of the magnetization curves for the same ferrofluid taken at different levels of dilution. The particle-size distribution was represented by the assumed form

$$p(x) = \frac{x^{\alpha}\exp(-x/x_0)}{x_0^{\alpha+1}\Gamma(\alpha+1)}, \tag{6}$$

where α and x_0 are fitted parameters, and $\Gamma(z)$ is the gamma function. Of all the theories tested, only one gave consistent results for the parameters determined by independent fitting of the magnetization curves at different concentrations—the so-called second-order modified mean-field (MMF2) theory of Ivanov and Kuznetsova [22,23]. The MMF2 expressions are as follows:

$$M(H) = \rho\left\langle \mu(x) L\left(\frac{\mu_0\mu(x)H_{\rm eff}}{k_{\rm B}T}\right)\right\rangle, \tag{7}$$

$$H_{\rm eff} = H + \frac{1}{3}M_{\rm L}(H) + \frac{1}{144}M_{\rm L}(H)\frac{dM_{\rm L}(H)}{dH}, \tag{8}$$

$$\chi = \chi_{\rm L}\left(1 + \frac{1}{3}\chi_{\rm L} + \frac{1}{144}\chi_{\rm L}^2\right). \tag{9}$$

Note that the effective field contains the Langevin magnetization and not the magnetization itself, and so the MMF2 equations are not transcendental. Essentially, the MMF2 theory arises from using the Yvon-Born-Bogolyubov-Green-Kirkwood (YBBGK) hierarchy [24] to relate the one-particle orientational distribution function (ODF) to the pair-correlation function (PCF) between particles, and then estimating the PCF with a perturbation expansion in the concentration ρ and the strength of the dipole-dipole interactions. The one-particle ODF then trivially gives the magnetization curve, and from that the initial susceptibility. The strength of the dipole-dipole interactions as compared to the thermal energy is measured by a dipolar coupling constant

$$\lambda = \frac{\mu_0\langle\mu^2(x)\rangle}{4\pi k_{\rm B}T\langle\sigma^3(x)\rangle} \tag{10}$$

in terms of which the Langevin susceptibility can be written

$$\chi_{\rm L} = 8\varphi\lambda. \tag{11}$$

The MMF2 expression for χ includes the exact terms in an expansion in terms of $\chi_{\rm L}$ up to order $\chi_{\rm L}^3 \sim \rho^3\lambda^3$, which of course does not refer specifically to a particular $p(x)$. This is a feature of several of the aforementioned theories [5–10,13,14,22,23]. The MMF2 expression is quite accurate for ferrofluids with $\chi \lesssim 5$ [20,21], while density-functional theory has been shown to work for $\chi \lesssim 4$ [17–19]. Note that in recent work by Szalai *et al.*, a thermodynamic perturbation theory for monodisperse ferrofluids was proposed that is accurate for dense ferrofluids with $\chi \lesssim 80$ [12]. This theory also yields good predictions for the magnetization curve and the nonlinear susceptibility, and reasonable predictions for the compressibility factor. Its accuracy relies on the pair distribution function of the hard-sphere fluid obtained from MC simulations, and as such the theory is not yet applicable to real polydisperse ferrofluids.

Concentrated magnetite ferrofluids with very high magnetic susceptibilities $\chi \sim 120$–150 at low temperatures down to $T \sim 200$ K have recently been synthesized [25–29], and these pose a significant challenge to the theories currently available. The high susceptibility is thought to arise from large particle-size polydispersity, and in particular to the strong dipole-dipole interactions between the largest particles. Therefore, an essential task is to extend Eqs. (7)–(9) to include extra terms, particularly those of higher order in the dipolar coupling constant. This has already been carried out to some extent [30,31]. For instance, the leading-order correction to Eq. (9) gives

$$\chi = \chi_{\rm L}\left[1 + \frac{1}{3}\chi_{\rm L}\left(1 + \frac{\lambda^2\Lambda_0^2}{25}\right) + \frac{1}{144}\chi_{\rm L}^2\right], \tag{12}$$

where Λ_0 is a dimensionless number given by a complicated average over the particle-size distribution [31], which will be defined again in Sec. II B: $\Lambda_0 = 1$ for a monodisperse ferrofluid, and $\Lambda_0 \geqslant 1$ for a polydisperse ferrofluid. Equations (9) and (12) were tested against simulation results for model systems, and it was shown that the extra term proportional to Λ_0^2 was essential to capture an enhancement in χ with increasing polydispersity [30]. Very recently, a further extension of Eq. (12) was tested against experimental measurements of χ in a dense, high-susceptibility ferrofluid [32]. This extended theory gives for the initial susceptibility an expression of the form

$$\chi = \chi_{\rm L}\left[1 + \frac{1}{3}\chi_{\rm L}\left(1 + \frac{\lambda^2\Lambda_0^2}{25}\right) + \frac{1}{144}\chi_{\rm L}^2(1 + \text{const} \times \lambda)\right], \tag{13}$$

where "const" once again depends on complicated averages over $p(x)$, and the theory is correct up to terms of order $\rho^3\lambda^4$. The extended theory was shown to be capable of describing the ferrofluid properties over the experimental temperature range, although the apparent particle-size distribution was determined by matching theory to the saturation magnetization $M(\infty)$ and χ at $T = 295$ K, and not through a full analysis of the magnetization curve because the corresponding extensions of Eqs. (7) and (8) were not yet available.

The idea that including more terms in the expansions of χ will improve results needs some discussion. For systems with hard-core interactions, the virial expansions of thermodynamic functions tend to converge with increasing orders of ρ; the virial coefficients can change sign, but generally the magnitudes of successive corrections decrease, and high-order virial expansions can be accurate even at very high densities [24]. The expansions in λ are more problematic, especially when applied to real polydisperse ferrofluids. The dipolar coupling constants for large particles are far beyond where such expansions are expected to work, and so the addition of extra terms is not guaranteed to give better results. Nonetheless, as will be shown in this work, large-particle fractions make very significant contributions to the magnetic properties of polydisperse ferrofluids, and so some attempt must be made to include the effects of strong dipolar interactions. It should be noted, though, that with high values of the dipolar coupling constant, including one extra term can lead to substantial deviations, and of either sign. This also applies to monodisperse ferrofluids characterized by a single, large dipolar coupling constant.

The main aims of the current work are twofold. First, the theory will be completed by determining the full expression for the magnetization curve corresponding to the initial-susceptibility expression given in Eq. (13). Second, the theory will be tested critically against simulation results for monodisperse, bidisperse, and polydisperse model ferrofluids with saturation magnetizations and Langevin susceptibilities up to those of recently synthesized concentrated ferrofluids. The results of this work, therefore, characterize the most advanced theoretical framework for analysis of highly concentrated, high-susceptibility ferrofluids. The rest of the article is organized as follows. The model, theory, and simulations are detailed in Sec. II. Two sets of results are discussed in detail: first, theoretical and simulation results for a polydisperse ferrofluid with a realistic particle-size distribution are compared to those for a monodisperse ferrofluid with the same saturation magnetization and Langevin susceptibility; and second, the corresponding results for a bidisperse ferrofluid with fractions of "small" and "large" particles. Section IV concludes the article.

II. MODEL, THEORY, AND SIMULATIONS

A. Model

The ferrofluid is modeled as a fluid of N dipolar hard spheres (DHSs) with magnetic-core diameter x, nonmagnetic layer thickness δ, hard-sphere diameter $\sigma = x + 2\delta$, and magnetic dipole moment $\mu = \pi x^3 M_s/6$. In both theory and simulation, the demagnetization fields are set equal to zero: in theory this is achieved by considering the fluid in a cylindrical container with infinite aspect ratio and volume V oriented in the same direction as an external magnetic field; in simulations this is achieved by using Ewald summations with conducting boundary conditions. For particle i, the position vector is $\boldsymbol{r}_i$ and the dipole moment is $\boldsymbol{\mu}_i = \mu_i(\sin\omega_i\cos\xi_i, \sin\omega_i\sin\xi_i, \cos\omega_i)$. The interaction energy between two DHSs i and j is

$$u(i,j) = u_s(i,j) + u_d(i,j), \tag{14}$$

the components of which are the short-range, hard-sphere potential

$$u_s(i,j) = \begin{cases} \infty, & r_{ij} < \sigma_{ij}, \\ 0, & r_{ij} \geqslant \sigma_{ij} \end{cases} \tag{15}$$

and the dipole-dipole interaction potential

$$u_d(i,j) = \frac{\mu_0}{4\pi}\left[\frac{(\boldsymbol{\mu}_i\cdot\boldsymbol{\mu}_j)}{r_{ij}^3} - \frac{3(\boldsymbol{\mu}_i\cdot\boldsymbol{r}_{ij})(\boldsymbol{\mu}_j\cdot\boldsymbol{r}_{ij})}{r_{ij}^5}\right], \tag{16}$$

where $\boldsymbol{r}_{ij} = \boldsymbol{r}_j - \boldsymbol{r}_i$ is the center-center separation vector, $r_{ij} = |\boldsymbol{r}_{ij}|$, and $\sigma_{ij} = (\sigma_i + \sigma_j)/2$. In the presence of an external uniform magnetic field H, the total interaction energy in units of the thermal energy $k_B T = \beta^{-1}$ is

$$\beta U = \sum_{i=1}^{N-1}\sum_{j>i}^{N}\beta u(i,j) - \sum_{i=1}^{N}\alpha_i\cos\omega_i, \tag{17}$$

where $\alpha_i = \beta\mu_0\mu_i H$ is the Langevin parameter for particle i.

B. Modified mean-field theory

In Refs. [22,23] it was shown that, in general, the effective field $H_{\rm eff}$ is determined by a single-particle potential of mean force (PMF) $-k_B T\Psi(\omega_1)$, where ω_1 is the polar angle between the dipole vector on a particle 1 and the external magnetic field. $\Psi(\omega_1)$ can be represented as an expansion in Legendre polynomials:

$$\Psi(\omega_1) = \sum_{k=0}^{\infty} a_k P_k(\cos\omega_1). \tag{18}$$

The first Legendre polynomial is $P_1 = \cos\omega_1$, just like the Zeeman term in Eq. (17), and the remaining terms can be omitted [22,23]. Therefore,

$$\Psi(\omega_1) = a_1\cos\omega_1 = \left(\frac{\mu_0\mu_1 H_{\rm eff}}{k_B T}\right)\cos\omega_1, \tag{19}$$

where a_1 is the effective Langevin parameter for the particle. Using the YBBGK hierarchy, it is possible to express $\Psi(\omega_1)$ through the pair distribution function (PDF) $g(1,2)$ between particles 1 and 2. The result is [22,23]

$$\Psi(\omega_1) = \alpha_1\cos\omega_1 - \rho\left\langle\int d\omega_1\int d\boldsymbol{r}_{12}\int d\boldsymbol{\Omega}_2\frac{d\beta u_d(1,2)}{d\omega_1}g(1,2)\right\rangle_2. \tag{20}$$

Here $\int d\omega_1$ means the indefinite integral with respect to ω_1 [22], $\langle\cdots\rangle_2$ means an average over the size of particle 2 according to Eq. (3), and $\int d\boldsymbol{\Omega}_i\ldots$ means a Boltzmann-weighted integration over the orientation of particle i with

$$d\boldsymbol{\Omega}_i = \frac{\alpha_i}{4\pi\sinh\alpha_i}\exp(\alpha_i\cos\omega_i)\sin\omega_i d\omega_i d\xi_i \tag{21}$$

and $\int d\boldsymbol{\Omega}_i = 1$. Equation (20) involves integrals of the PDF $g(1,2)$ over all possible positions and orientations of particle 2. The PDF is calculated using the so-called λ expansion starting from the properties of a reference system [24]; a scaling parameter ϵ is used here instead to avoid confusion

with the dipolar coupling constant λ. The reference system is the hard-sphere fluid, and the perturbation is the dipole-dipole interaction energy $U_{\rm d} = \sum_{i<j} u_{\rm d}(i,j)$. The total interaction energy is written $U_{\rm s} + \epsilon U_{\rm d}$, where $\epsilon = 1$ corresponds to the system of interest. In the canonical ensemble, the n-particle distribution function is defined as [24]

$$g(1,2,\ldots,n) = \frac{1}{\rho^n}\frac{N!}{(N-n)!}\frac{\int d(n+1)\cdots\int dN\exp\left(-\beta U_{\rm s}-\epsilon\beta U_{\rm d}\right)}{\int d1\cdots\int dN\exp\left(-\beta U_{\rm s}-\epsilon\beta U_{\rm d}\right)}, \tag{22}$$

where $\int di = \int d\boldsymbol{r}_i \int d\boldsymbol{\Omega}_i$. In the present work, the PDF $g(1,2)$ is calculated up to second order in ϵ, with $\epsilon = 1$:

$$g(1,2) = g_{\rm s}(1,2) + \left[\frac{\partial g(1,2)}{\partial\epsilon}\right]_{\epsilon=0} + \frac{1}{2}\left[\frac{\partial^2 g(1,2)}{\partial\epsilon^2}\right]_{\epsilon=0}. \tag{23}$$

The derivatives are determined up to order ρ through standard calculations [24]; the details are summarized in Appendix A. The evaluation of the necessary terms up to order ρ that contribute to the parameter a_1 is outlined in Appendix B. The main point is that Eqs. (19) and (20) allow the identification of an effective field felt by particle 1, and the magnetization curve can be expressed in terms of this quantity as

$$M(H) = \rho\left\langle \mu_1 L\left(\frac{\mu_0\mu_1 H_{\rm eff}}{k_{\rm B}T}\right)\right\rangle_1. \tag{24}$$

The final expression for the effective field is

$$\begin{aligned} H_{\rm eff} = {} & H + \frac{1}{3}M_{\rm L}(H) + \frac{1}{144}M_{\rm L}(H)\frac{dM_{\rm L}}{dH} \\ & + \frac{\mu_0\rho}{75}\left(\frac{\mu_1}{k_{\rm B}T}\right)^2\left\langle\frac{\mu_2^3 L(\alpha_2)}{\sigma_{12}^6}\right\rangle_2 \\ & + \frac{1}{4\pi\langle\sigma^3\rangle}\left(\frac{\mu_0\rho}{k_{\rm B}T}\right)^2\left\langle\mu_2^3 L(\alpha_2)\left[\frac{71}{72\,000}\mu_1^2 A(\sigma_1,\sigma_2,\sigma_3)\right.\right. \\ & \left.\left. + \frac{(3\ln 2-7)}{360}\mu_3^2\frac{L(\alpha_3)}{\alpha_3}B(\sigma_1,\sigma_2,\sigma_3)\right]\right\rangle_{2,3}, \end{aligned} \tag{25}$$

where $\langle\cdots\rangle_{2,3}$ means averages over the sizes of both particles 2 and 3 according to Eq. (3). The coefficients A and B are complicated geometrical factors involving integrals over the hard-sphere diameters,

$$\begin{aligned} A(\sigma_1,\sigma_2,\sigma_3) = {} & \frac{120\langle\sigma^3\rangle}{71}\int_{\sigma_{12}}^{\sigma_{12}+\sigma_3}\frac{dr_{12}}{r_{12}^8}(\sigma_{13}+\sigma_{23}-r_{12})^2 \\ & \times[r_{12}(r_{12}+2\sigma_{13}+2\sigma_{23}-3(\sigma_{13}-\sigma_{23})^2], \end{aligned} \tag{26}$$

$$\begin{aligned} & B(\sigma_1,\sigma_2,\sigma_3) \\ & = \frac{36\langle\sigma^3\rangle}{3\ln 2-7}\left[\int_{\sigma_{12}}^{\sigma_{12}+\sigma_3} dr_{12}\int_{\sigma_{23}}^{r_{12}+\sigma_{13}} dr_{23}C(r_{12},r_{23})\right. \\ & \left. + \int_{\sigma_{12}+\sigma_3}^{\infty} dr_{12}\int_{r_{12}-\sigma_{13}}^{r_{12}+\sigma_{13}} dr_{23}C(r_{12},r_{23})\right], \end{aligned} \tag{27}$$

$$C(r_{12},r_{23}) = \frac{\left(r_{12}^2+r_{23}^2-\sigma_{13}^2\right)^3}{4r_{12}^4 r_{23}^7} - \frac{r_{12}^2+r_{23}^2-\sigma_{13}^2}{r_{12}^2 r_{23}^5}. \tag{28}$$

Factors of $\langle\sigma^3\rangle$ are included in Eqs. (25)–(27) so that, in the monodisperse case, $A = B = 1$. Finally, the expression for the initial susceptibility is

$$\begin{aligned} \chi = {} & \chi_{\rm L}\left\{1 + \frac{1}{3}\chi_{\rm L}\left(1+\frac{\lambda^2\Lambda_0^2}{25}\right) + \frac{1}{144}\chi_{\rm L}^2\right. \\ & \left. + \chi_{\rm L}^2\lambda\left[\frac{71\Lambda_1}{24\,000} + \frac{(3\ln 2-7)\Lambda_2}{360}\right]\right\}. \end{aligned} \tag{29}$$

The coefficients Λ_0, Λ_1, and Λ_2 are related to averages of the magnetic-core and hard-sphere diameters over the particle-size distribution,

$$\Lambda_0 = \frac{\langle\sigma\rangle^3}{\langle x^6\rangle^2}\sqrt{\left\langle\frac{x_1^{12}x_2^{12}}{\sigma_{12}^6}\right\rangle_{1,2}}, \tag{30}$$

$$\Lambda_1 = \frac{\left\langle x_1^{12}x_2^{12}A(\sigma_1,\sigma_2,\sigma_3)\right\rangle_{1,2,3}}{\langle x^6\rangle^4}, \tag{31}$$

$$\Lambda_2 = \frac{\left\langle x_1^6 x_2^{12}x_3^6 B(\sigma_1,\sigma_2,\sigma_3)\right\rangle_{1,2,3}}{\langle x^6\rangle^4}. \tag{32}$$

Note that all of the coefficients A, B, Λ_0, Λ_1, and Λ_2 are defined so that they are equal to 1 in the monodisperse case; the expressions for the effective field and initial susceptibility are then somewhat simpler than those in the polydisperse case. The initial susceptibility becomes

$$\begin{aligned} \chi = {} & \chi_{\rm L}\left[1 + \frac{1}{3}\chi_{\rm L}\left(1+\frac{\lambda^2}{25}\right) + \frac{1}{144}\chi_{\rm L}^2\right. \\ & \left. + \chi_{\rm L}^2\lambda\left(\frac{71}{24\,000} + \frac{3\ln 2-7}{360}\right)\right]. \end{aligned} \tag{33}$$

This shows that the correction term $\propto\chi_{\rm L}^2\lambda^2$ is positive while the term $\propto\chi_{\rm L}^3\lambda$ is negative. Note that this combination of terms decreases the susceptibility of concentrated, high-susceptibility, monodisperse ferrofluids (for which $\chi_{\rm L}$ is large). In this work, it is shown that the corresponding terms for polydisperse ferrofluids with a wide range of parameters lead to a net increase in χ. Equations (24), (25), and (29) will be referred to as the MMF2+ predictions.

These results are in no way optimized for a particular particle-size distribution. Although the Γ distribution (6) is mathematically convenient, and will be used in what follows, any other physically reasonable distribution, such as the log-normal distribution, will give similar results. What is important is the breadth of the particle-size distribution, and whether there is a significant fraction of large particles with strong dipolar interactions. This is shown explicitly by considering a polydisperse ferrofluid with a Γ distribution of particle sizes, bidisperse ferrofluids with small-particle and large-particle fractions, and a monodisperse ferrofluid. These different systems are detailed in the next section.

TABLE I. Particle-size distributions in the ferrofluids studied in this work. x is the magnetic-core diameter, N_i is the number of particles in a fraction, and λ is the dipolar coupling constant for magnetite particles at $T = 295$ K. For each fraction, $\lambda = \mu_0\mu^2/4\pi k_B T\sigma^3$, where $\mu = \pi x^3 M_s/6$ is the dipole moment on a particle, and $\sigma = x + 4$ nm is the hard-sphere diameter. The bottom row gives the average dipolar coupling constant (10).

	Monodisperse			Bidisperse 1			Bidisperse 2			Polydisperse		
Fraction	N_i	x/nm	λ	N_i	x/nm	λ	N_i	x/nm	λ	N_i	x/nm	λ
1	500	13.934758	1.97	380	11.434970	0.943	470	9.974882	0.560	4	3	0.00330
2				120	16.008959	3.26	30	18.841444	5.82	38	5	0.0332
3										100	7	0.137
4										129	9	0.375
5										108	11	0.814
6										66	13	1.52
7										33	15	2.58
8										14	17	4.04
9										5	19	6.00
10										3	21	8.51
Average			1.97			1.89			1.71			1.74

C. Computer simulations

Four different simulation configurations were studied, as detailed in Table I, all with a total of $N = 500$ particles. A polydisperse ferrofluid was studied with a discretized version of the particle-size distribution in Eq. (6) with $\alpha = 9$ and $x_0 = 1$ nm; these are typical numbers for the concentrated, high-susceptibility, polydisperse ferrofluids that have been synthesized recently. The procedure for discretizing $p(x)$ was described in Ref. [20]. The fluid was represented by 10 fractions with magnetic-core diameters $x = 3,5,7,\ldots,21$ nm, and the number of particles in each fraction is given in Table I. The discretization procedure is designed to minimize the difference between the discretized and the exact averages,

$$\langle x^n\rangle = x_0^n \prod_{k=1}^{n}(\alpha + k). \tag{34}$$

The deviations of the first six discretized averages are +0.00% ($n = 1$), +0.28% ($n = 2$), +0.63% ($n = 3$), +0.84% ($n = 4$), +0.64% ($n = 5$), and −0.26% ($n = 6$); these are insignificant. The discretized and exact magnetic-core polydispersity indices $s = \sqrt{\langle x^2\rangle - \langle x\rangle^2}/\langle x\rangle$ are 0.321 and 0.316, respectively. The hard-sphere diameter of each fraction is $\sigma = x + 4$ nm. For magnetite particles ($M_s = 4.8 \times 10^5$ A m^{-1}) at $T = 295$ K, the dipolar coupling constants for the separate fractions are in the range $0.003\,30 \leqslant \lambda \leqslant 8.51$, and the average dipolar coupling constant as given by Eq. (10) is $\lambda = 1.74$. The polydisperse ferrofluid was simulated at four different concentrations corresponding to saturation magnetizations $M(\infty) =$ 25, 50, 75, and 100 kA m^{-1}. The corresponding magnetic volume fractions (5), Langevin susceptibilities (2) and (11), number concentrations, and hard-sphere volume fractions (4) are given in Table II.

The results for the polydisperse ferrofluid were compared with those for a monodisperse ferrofluid with the same saturation magnetizations and the same Langevin susceptibilities at $T = 295$ K; the corresponding value of the dipolar coupling constant is $\lambda = 1.97$. The magnetic-core diameter and concentrations are given in Tables I and II, respectively.

Finally, two different bidisperse ferrofluids were studied at a single concentration with a saturation magnetization $M(\infty) = 75$ kA m^{-1}: bidisperse configuration 1, with $s =$ 0.156 and containing 24% of large particles with $\lambda = 3.26$; and bidisperse configuration 2, with $s = 0.200$, containing 6% of large particles with $\lambda = 5.82$. Both configurations contain small particles with $\lambda < 1$. The details are given in Tables I and II.

It is emphasized that the monodisperse, bidisperse, and polydisperse systems are designed so that, for a given saturation magnetization and temperature, they have the same Langevin susceptibility. The aim is to concentrate on deviations from the MMF2 theory, which depends only on χ_L. For each configuration and concentration, two sets of calculations were performed: the full magnetization curve $M(H)$ at $T = 295$ K, and the initial susceptibility χ over the temperature range $0.75 \leqslant T/295\ \text{K} \leqslant 1.10$. In all cases, the comparison with theoretical results for bidisperse and polydisperse ferrofluids is for the precise particle-size distributions used in the simulations, as detailed in Table I.

MC simulations were carried out in the canonical (NVT) ensemble in a cubic simulation cell with periodic boundary conditions applied. The long-range dipole-dipole interactions were computed using the Ewald summation with conducting boundary conditions. Translational and orientational moves were attempted separately with maximum displacements set to achieve acceptance rates of 20% and 50%, respectively. The initial susceptibility was computed using the fluctuation formula

$$\chi = \frac{\mu_0\langle|\boldsymbol{M}|^2\rangle}{3Vk_BT}, \tag{35}$$

where $\boldsymbol{M} = \sum_{i=1}^{N}\boldsymbol{\mu}_i$ is the instantaneous magnetization. After equilibration, some extremely long production runs were carried out, with up to 2.5×10^7 attempted MC moves per particle. Estimates of statistical errors were calculated using the blocking procedure described in Ref. [33].

TABLE II. Magnetic properties of the ferrofluids studied in this work. $M(\infty)$ is the saturation magnetization of the ferrofluid, φ_m is the magnetic volume fraction (5), χ_L is the Langevin susceptibility (2) and (11), ρ is the number concentration, and φ is the hard-sphere volume fraction (4).

			Monodisperse		Bidisperse 1		Bidisperse 2		Polydisperse	
$M(\infty)$/kA m^{-1}	φ_m	χ_L	$\rho/10^{23}$ m^{-3}	φ	$\rho/10^{23}$ m^{-3}	φ	$\rho/10^{23}$ m^{-3}	φ	$\rho/10^{23}$ m^{-3}	φ
25	0.052083	1.748484	0.367622	0.111042					0.748827	0.125315
50	0.104167	3.496968	0.735245	0.222084					1.497655	0.250630
75	0.156250	5.245452	1.102867	0.333126	1.406917	0.347501	2.236566	0.384171	2.246482	0.375944
100	0.208333	6.993935	1.470489	0.444168					2.995310	0.501259

III. RESULTS

A. Polydisperse ferrofluid

Figure 1 shows the magnetization curves of monodisperse and polydisperse ferrofluids at $T = 295$ K over a broad range of external magnetic fields $0 \leqslant H \leqslant 100$ kA m^{-1}, as measured in MC simulations, and from the MMF2 and MMF2+ theories. In general, for each concentration, the magnetization curve for the monodisperse ferrofluid has a sharper change in slope at moderate field strengths than that for the polydisperse ferrofluid. This is because in the monodisperse ferrofluid, all of the particles respond equally to the field, while in the polydisperse ferrofluid the larger particles should be aligned first, and the smaller particles will only be aligned at very high field strengths. This explains the more gradual approach to $M(\infty)$ in the results for the polydisperse ferrofluid. At the three lowest concentrations—$M(\infty) = 25$, 50, and 75 kA m^{-1}—the MMF2 and MMF2+ predictions for each system are barely distinguishable. At the highest

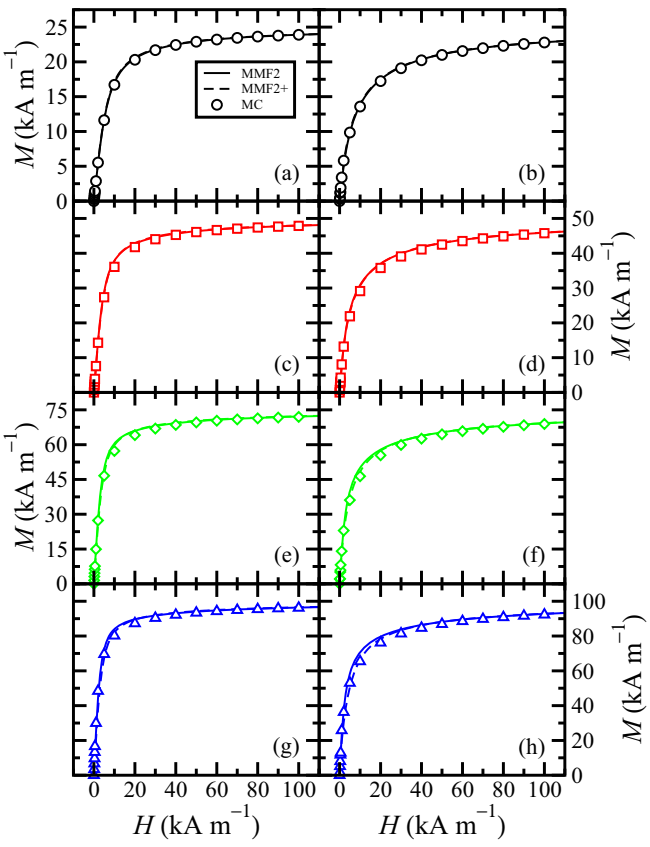

FIG. 1. Full magnetization curves of monodisperse [(a), (c), (e), and (g)] and polydisperse [(b), (d), (f), and (h)] ferrofluids at $T = 295$ K and various concentrations: (a) and (b) $M(\infty) = 25$ kA m^{-1}; (c) and (d) $M(\infty) = 50$ kA m^{-1}; (e) and (f) $M(\infty) = 75$ kA m^{-1}; and (g) and (h) $M(\infty) = 100$ kA m^{-1}. The points are from MC simulations, the solid lines are from MMF2 theory, and the dashed lines are from MMF2+ theory.

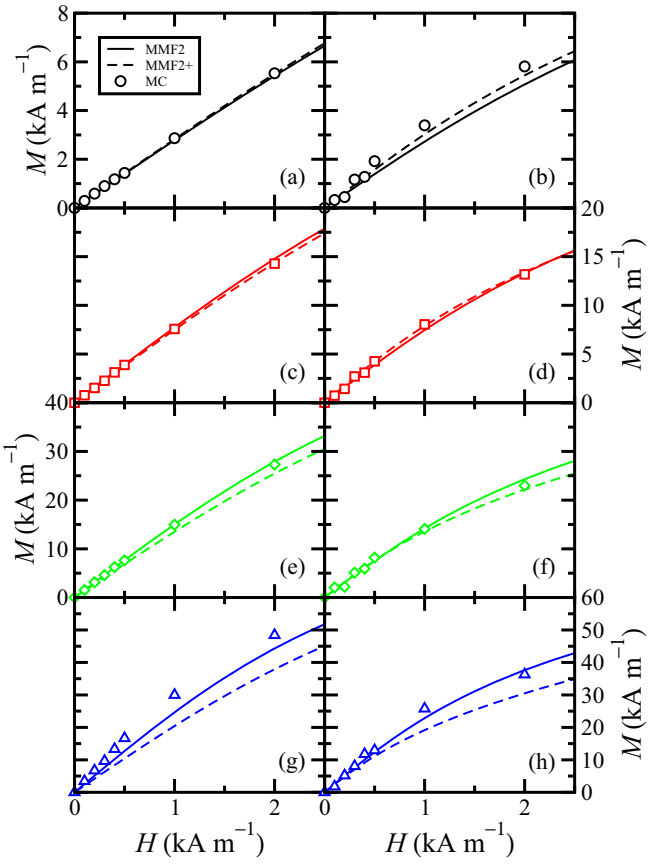

FIG. 2. Low-field magnetization curves of monodisperse [(a), (c), (e), and (g)] and polydisperse [(b), (d), (f), and (h)] ferrofluids at $T = 295$ K and various concentrations: (a) and (b) $M(\infty) = 25$ kA m^{-1}; (c) and (d) $M(\infty) = 50$ kA m^{-1}; (e) and (f) $M(\infty) = 75$ kA m^{-1}; and (g) and (h) $M(\infty) = 100$ kA m^{-1}. The points are from MC simulations, the solid lines are from MMF2 theory, and the dashed lines are from MMF2+ theory.

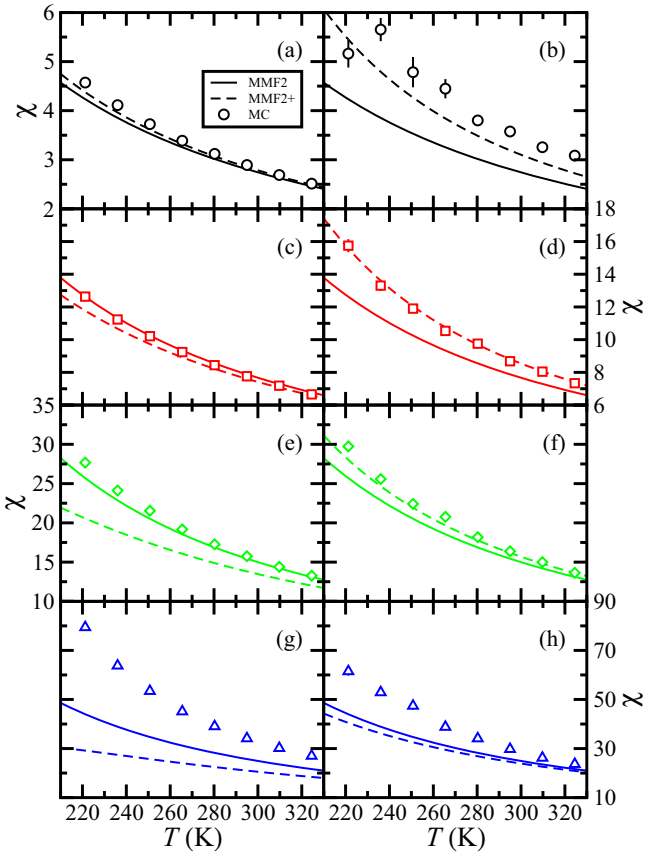

FIG. 3. Initial susceptibility as a function of temperature for monodisperse [(a), (c), (e), and (g)] and polydisperse [(b), (d), (f), and (h)] ferrofluids at various concentrations: (a) and (b) $M(\infty) = 25$ kA m^{-1}; (c) and (d) $M(\infty) = 50$ kA m^{-1}; (e) and (f) $M(\infty) = 75$ kA m^{-1}; and (g) and (h) $M(\infty) = 100$ kA m^{-1}. The points are from MC simulations, the solid lines are from MMF2 theory, and the dashed lines are from MMF2+ theory.

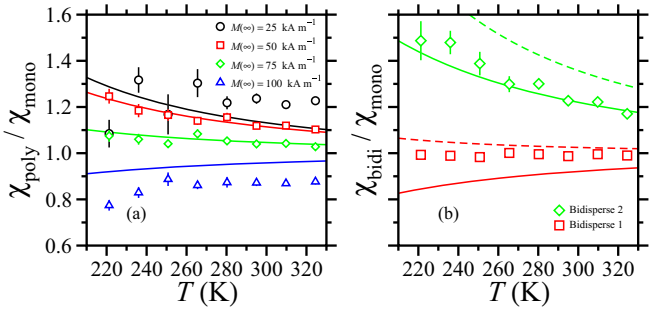

FIG. 4. The initial susceptibilities for (a) polydisperse and (b) bidisperse ferrofluids divided by those for monodisperse ferrofluids at various concentrations. The points are from MC simulations, the solid lines in (a) and (b) are from MMF2+ theory for the polydisperse/bidisperse ferrofluids and MMF2 theory for the monodisperse ferrofluids, and the dashed lines in (b) are from MMF2+ theory for all ferrofluids.

concentration—$M(\infty) = 100$ kA m^{-1}—the MMF2+ theory for the polydisperse ferrofluid gives a slightly lower value of M for moderate values of H than does the MMF2 theory, and this is in better agreement with simulations. Nonetheless, the differences are small, and so the low-H behavior will be examined in more detail next.

Figure 2 shows the same magnetization curves in the range $0.0 \leqslant H \leqslant 2.5$ kA m^{-1}. These data show linear behavior at low fields and the onset of nonlinear behavior with increasing H. The key point here is that the MMF2 theory appears to be slightly more accurate than the MMF2+ theory for the monodisperse ferrofluids with $M(\infty) = 25$, 50, and 75 kA m^{-1}, while MMF2+ works better for the polydisperse ferrofluids at the same concentrations. For both the monodisperse and polydisperse ferrofluids with $M(\infty) = 100$ kA m^{-1}, the MMF2 theory looks to be more accurate, but in fact the agreement is not very good in either case, as is shown next.

Figure 3 shows the initial susceptibilities of monodisperse and polydisperse ferrofluids over a broad temperature range $221.25 \leqslant T \leqslant 324.50$ K. Note that the MMF2 predictions are the same for the monodisperse and polydisperse ferrofluids, as they only depend on the value of χ_L, which is the same in both cases. For the monodisperse ferrofluid at low concentration [$M(\infty) = 25$ kA m^{-1}] the MMF2+ theory is a little closer to the simulation results than the MMF2 theory, but the differences are small. For the polydisperse ferrofluid at the same concentration, the MMF2+ theory is clearly better than the MMF2 theory, but there are still significant deviations from the simulation results. The simulation results show considerable scatter at low temperature, despite very long simulations; this will be explained below. At intermediate concentrations [$M(\infty) = 50$ and 75 kA m^{-1}] the MMF2 theory gives good predictions for the monodisperse ferrofluid, while the MMF2+ theory is reliable for the polydisperse ferrofluid. At the highest concentration [$M(\infty) = 100$ kA m^{-1}] neither theory works well: although the MMF2 theory is closer to the simulation results for both the monodisperse and polydisperse ferrofluids, the deviations at all but the highest temperatures are substantial. The overall theoretical trend for both the monodisperse and polydisperse ferrofluids is that at low concentration, the MMF2+ susceptibility is higher than the MMF2 one, and that with increasing concentration the order is reversed, with the crossover occurring at lower concentration in the monodisperse case.

As a further comparison between monodisperse and polydisperse ferrofluids, Fig. 4(a) shows the ratio of the initial susceptibilities, χ_{poly}/χ_{mono}. The MC simulation results show that: (i) χ_{poly}/χ_{mono} approaches 1 with increasing temperature as the dipolar coupling constants decrease and the Langevin susceptibility decreases; and (ii) for a given temperature, χ_{poly}/χ_{mono} decreases with increasing concentration, starts from a value greater than 1 at low concentration, and becomes less than 1 between $M(\infty) = 75$ and 100 kA m^{-1}. The latter observation agrees with results for four-fraction ferrofluids with $\varphi_m \leqslant 0.119$ [or $M(\infty) \leqslant 57$ kA m^{-1}], where χ_{poly}/χ_{mono} decreases with increasing φ_m. Now, a glance at Fig. 3 shows that the MMF2+ prediction is $\chi_{poly}/\chi_{mono} > 1$ at all concentrations, and moreover the ratio increases with increasing concentration, which clearly is not correct. MMF2 theory is more accurate for the monodisperse ferrofluids, and therefore the theoretical curves plotted in Fig. 4(a) are given by the ratio of MMF2+ theory (for the polydisperse ferrofluid)

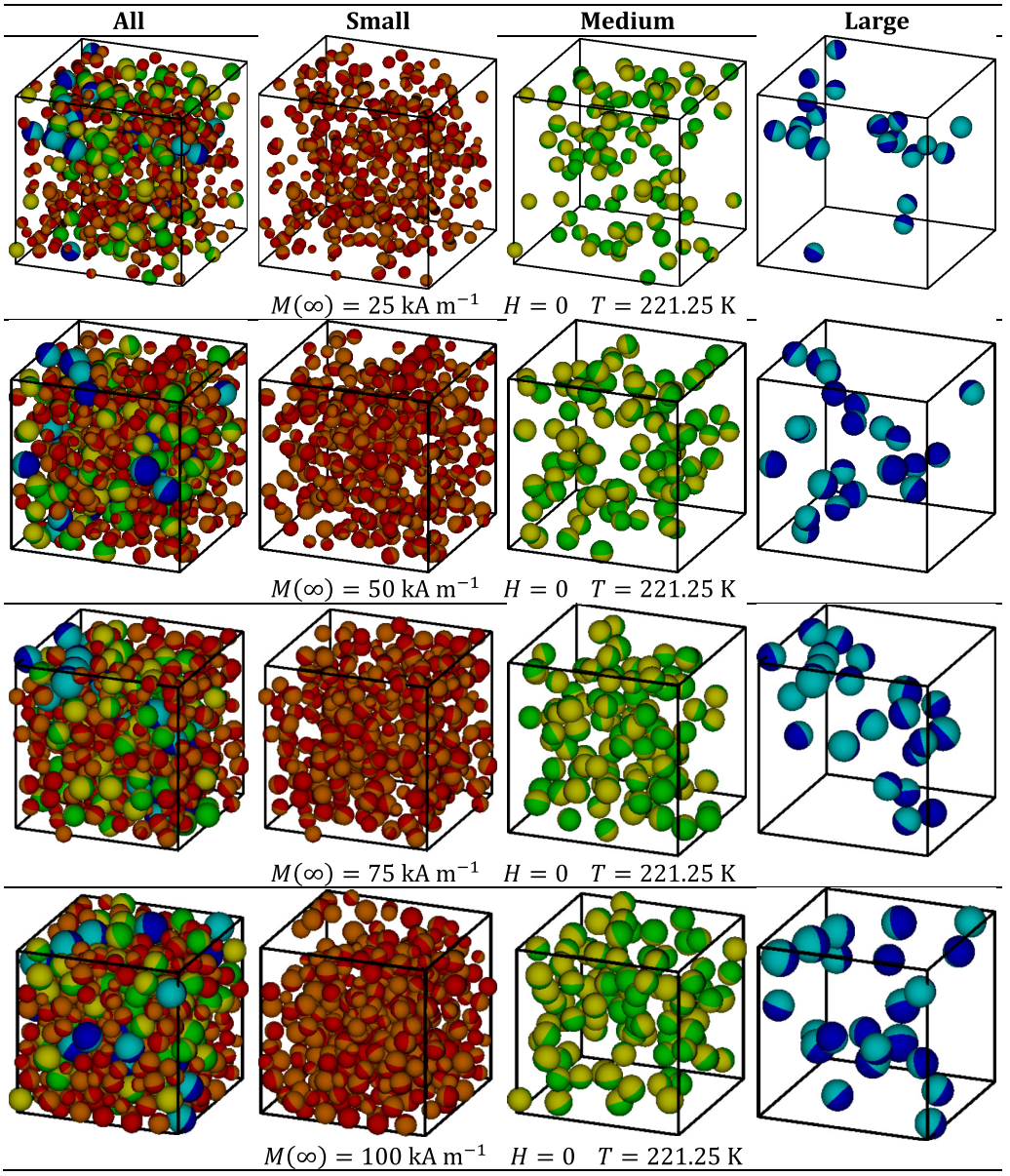

FIG. 5. Simulation snapshots for the polydisperse ferrofluid in zero field and at $T = 221.25$ K: (first row) $M(\infty) = 25$ kA m^{-1}; (second row) $M(\infty) = 50$ kA m^{-1}; (third row) $M(\infty) = 75$ kA m^{-1}; (fourth row) $M(\infty) = 100$ kA m^{-1}. The first column shows all of the particles, the second column shows the small particles, the third column shows the medium particles, and the fourth column shows the large particles.

and the MMF2 theory (for the monodisperse ferrofluid). These curves show reasonable agreement with simulations at $M(\infty) = 50$ and 75 kA m^{-1}, but they deviate from the results at $M(\infty) = 25$ and 100 kA m^{-1}, as per the results in Fig. 3.

To provide microscopic insight into these trends, Fig. 5 shows some simulation snapshots of the systems at low temperature ($T = 221.25$ K) in zero external field. The particles have been divided up into three groups according to the dipolar coupling constants at $T = 295$ K listed in Table I: 379 "small" particles with $\lambda \leqslant 1$, 99 "medium" particles with $1 < \lambda \leqslant 4$, and 22 "large" particles with $\lambda > 4$. $\lambda > 4$ is roughly the region where nose-to-tail chainlike correlations between dipoles are expected to become important in low-concentration ferrofluids [34]. The snapshots show that at low temperature and at all concentrations, the large particles are aggregated, although not in well-defined separate chains, and so a cluster distribution will not be very informative. Instead, Figs. 6 and 7 show the radial distribution functions (RDFs) $g(r)$ and the static structure factors $S(q)$, respectively, calculated *separately* for each of the small-, medium-, and large-particle groups at low temperature ($T = 221.25$ K) and at infinite temperature ($\lambda = 0$) in zero external field. The purpose of this comparison is to see how much structure there is in the system due to strong dipolar interactions as compared to hard-sphere interactions alone. Results are shown from both computer simulations and the theory at the MMF2+ level. In the simulations, $g(r)$ was calculated in the usual way [33], while the structure factor was calculated using the explicit reciprocal-space sum $S(\boldsymbol{q}) = N^{-1}\langle\rho(\boldsymbol{q})\rho(-\boldsymbol{q})\rangle$, where $\rho(\boldsymbol{q}) = \sum_{j=1}^{N} \exp(-i\boldsymbol{q}\cdot\boldsymbol{r}_j)$, and results for equal $q = |\boldsymbol{q}|$ were averaged. The theoretical

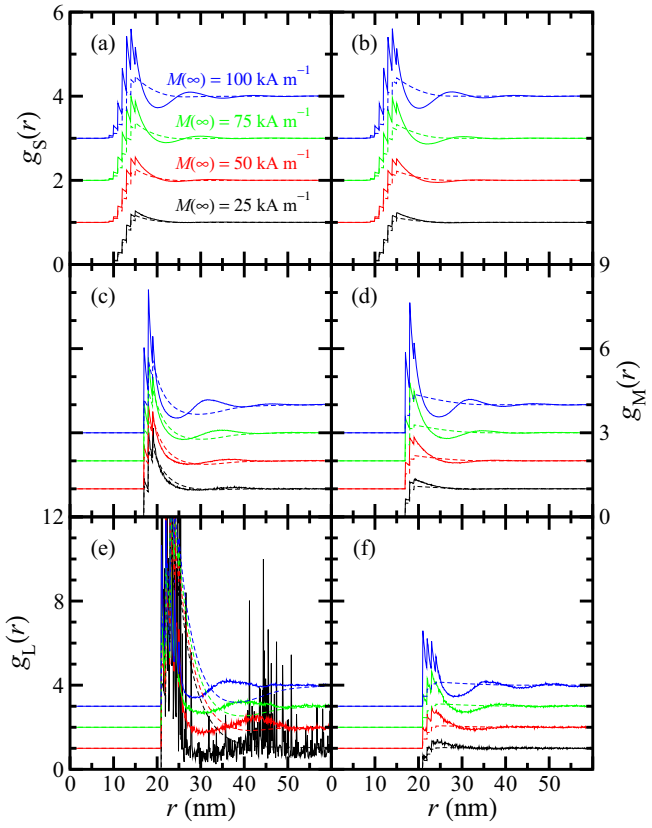

FIG. 6. Radial distribution functions of polydisperse ferrofluids at (a),(c),(e) $T = 221.25$ K; and (b),(d),(f) $T = \infty$, and various concentrations: (a) and (b) small (S) particles; (c) and (d) medium (M) particles; and (e) and (f) large (L) particles. Results are shown for $M(\infty) = 25$, 50, 75, and 100 kA m^{-1} as indicated, and they are separated from one another by one unit for clarity. Simulation results are shown as solid lines, and the MMF2+ predictions are shown as dashed lines.

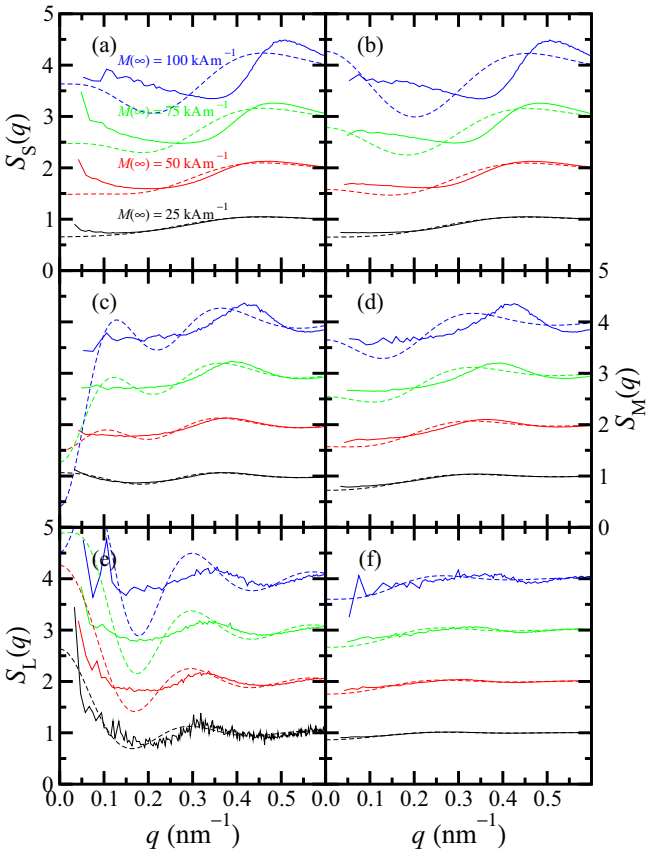

FIG. 7. Static structure factors of polydisperse ferrofluids at (a), (c), (e) $T = 221.25$ K; and (b), (d), (f) $T = \infty$, and various concentrations: (a) and (b) small (S) particles; (c) and (d) medium (M) particles; (e) and (f) large (L) particles. Results are shown for $M(\infty) = 25$, 50, 75, and 100 kA m^{-1} as indicated, and they are separated from one another by one unit for clarity. Simulation results are shown as solid lines, and the MMF2+ predictions are shown as dashed lines.

expression for $g(r)$ in zero field is detailed in Appendix B, and $S(q) = 1 + 4\pi\rho \int_0^\infty dr\, r^2[\sin(qr)/qr][g(r) - 1]$ was determined by numerical integration.

Considering the simulation results first, Fig. 6 shows that all of the RDFs develop larger primary and secondary peaks with increasing concentration, as measured by $M(\infty)$. The fine structure corresponds to the differences between the discretized hard-core diameters in each fraction. The small-particle RDFs are insensitive to temperature, since the dipolar coupling constants are low even at low temperature. The medium-particle RDFs are more sensitive to temperature due to the stronger dipolar interactions. The large-particle RDFs show very strong clustering at low temperature—although the data are very noisy—and only moderate ordering at high temperature. These trends are mirrored in the static structure factor, shown in Fig. 7. Again, the results for the small-particle and medium-particle fractions are much less sensitive to temperature than those for the large-particle fraction. $S(q)$ for the large particles at low temperature and low concentration shows the familiar small-q increase expected for chainlike correlations [35]; turning off the dipolar interactions leads to an almost total disappearance of nontrivial structure. The extent of large-particle clustering decreases with increasing concentration, showing that the hard-sphere correlations become more important. These results confirm that, overall, the dipole-dipole interactions between the large particles give rise to clustering, while the small and medium particles remain disordered. The presence of large-particle clusters is responsible for the imperfect convergence of the MC simulations: it takes a long time for magnetization fluctuations of clusters to relax. Nonetheless, the particles do not aggregate irreversibly, the clusters continue to evolve (albeit slowly), and so the suspension has not coagulated. The ferrofluid is therefore a stable colloidal suspension.

The comparison between theory and simulation gives some useful insights. The agreement between theory and simulation is quite good at low concentration, but worsens with increasing concentration due to the truncation of $g(r)$ to terms of order ρ. For the same reason, the predicted small-q behavior of $S(q)$ is inaccurate because of the omission of long-range correlations mediated by two or more particles in between a chosen pair of particles [36,37]. The theory gets right the general increase in structure with decreasing temperature, but the details are wrong because of the truncation of the expansion in λ. For the

large particles in systems with $M(\infty) \leqslant 75\,\mathrm{kA\,m^{-1}}$, the theory does quite well in predicting the strong increase in structure with decreasing temperature; this is easier to see in the results for $S(q)$, as the simulation results for $g(r)$ are very noisy.

These results shed some light on the reasons for the relative performance of each theory in predicting the properties of the polydisperse ferrofluid. At low concentrations, the magnetic properties of the polydisperse ferrofluid are strongly influenced by the dipole-dipole interactions between the large particles. To describe the orientational correlations arising from these interactions would require a large number of terms in the expansion in λ, but both MMF theories are truncated at low order. At high concentrations, the structural properties of the ferrofluid are dictated by the hard-sphere interactions, but the MMF2 and MMF2+ theories are truncated at low order in ρ, and so they do not give an accurate representation of the hard-sphere reference system. At intermediate concentrations, neither the hard-sphere correlations nor the dipolar chainlike correlations between large particles are so pronounced, and so it seems that the MMF2+ theory is able to give a reasonable account of both within a perturbative scheme. In fact, the phenomenon of strong dipolar correlations between large particles having a greater effect at low concentration than at high concentration has been seen before in the context of centrifugal sedimentation and separation of small and large particles in ferrofluids [38]. The separation factor describing the segregation of small and large particles in strong effective gravitational fields is greater at low concentration than at high concentration, and this can be explained by the large particles forming distinct aggregates and sedimenting out at low concentration.

B. Bidisperse ferrofluid

The results from Sec. III A show that the MMF2 theory works well for the monodisperse ferrofluid, and MMF2+ works well for a polydisperse ferrofluid containing a significant fraction of "large" particles with $\lambda > 4$ that aggregate. To determine if this is a general feature, two bidisperse ferrofluids have been studied at a single concentration of $M(\infty) = 75\,\mathrm{kA\,m^{-1}}$, and with the same Langevin susceptibility as the corresponding monodisperse and polydisperse ferrofluids (see Table I). Bidisperse configuration 1 contains 24% of particles with $\lambda = 3.26$, which is not in the regime where strong cluster formation is expected. Bidisperse configuration 2 contains 6% of particles with $\lambda = 5.82$, which should form clusters.

Figure 8 shows the full magnetization curves for the monodisperse, bidisperse 1, and bidisperse 2 configurations at $T = 295$ K. A direct comparison of the simulation results [panel (a)] shows that, for a given magnetic field, the magnetization decreases with increasing polydispersity, i.e., from monodisperse, to bidisperse 1, to bidisperse 2. As for the monodisperse versus polydisperse case, large particles are easily oriented with the field, while small particles are only aligned at high magnetic fields. In all cases, the MMF2 and MMF2+ predictions are similar to each other [panels (b)–(d)] and generally in good agreement with the simulation results. In the case of bidisperse configuration 2, the MMF2+ curve is slightly lower than the MMF2 curve, and closer to the simulation results.

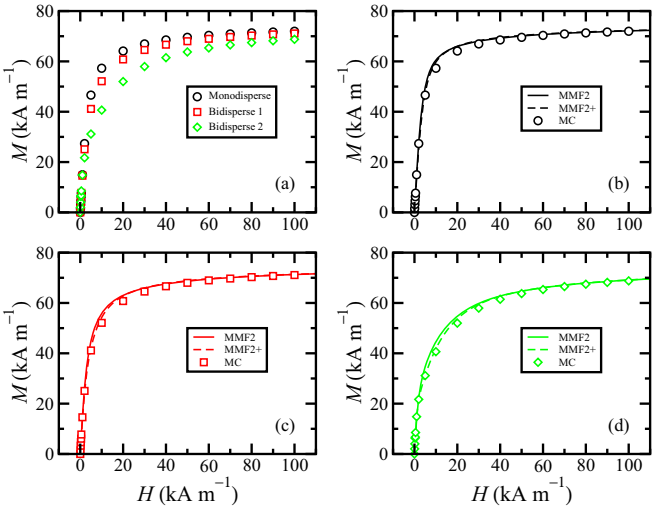

FIG. 8. Full magnetization curves of monodisperse and bidisperse ferrofluids at $T = 295$ K and with $M(\infty) = 75$ kA m^{-1}: (a) all simulation results; (b) monodisperse configuration; (c) bidisperse configuration 1; and (d) bidisperse configuration 2. The points are from MC simulations, the solid lines are from MMF2 theory, and the dashed lines are from MMF2+ theory.

Figure 9 shows the low-H behavior of the magnetization curves. Figure 9(a) shows all of the simulation results, along with the limiting linear slope calculated using Eq. (35), showing good consistency. The initial susceptibilities of the monodisperse configuration and bidisperse configuration 1 are very similar, while that of bidisperse configuration 2 is clearly much larger. The comparisons with theory [panels (b)–(d)] show that MMF2 theory works well for the monodisperse

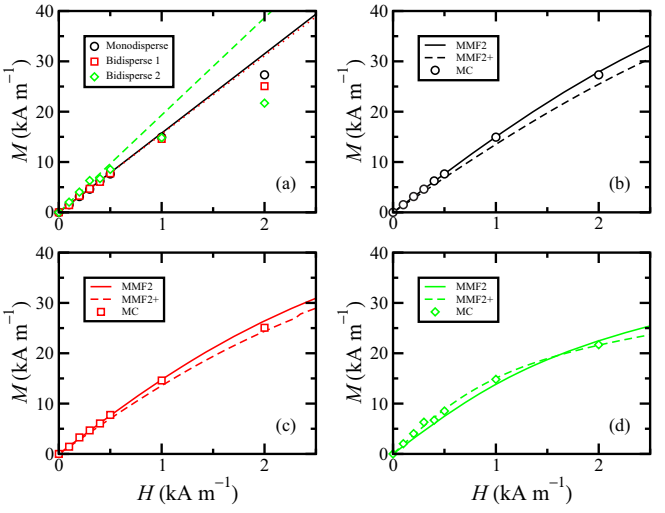

FIG. 9. Low-field magnetization curves of monodisperse and bidisperse ferrofluids at $T = 295$ K and with $M(\infty) = 75$ kA m^{-1}: (a) all simulation results; (b) monodisperse configuration; (c) bidisperse configuration 1; and (d) bidisperse configuration 2. The points are from MC simulations; in (a) the lines are the linear parts of the magnetization curves with the initial susceptibility calculated using Eq. (35), and in (b)–(d) the solid lines are from MMF2 theory and the dashed lines are from MMF2+ theory.

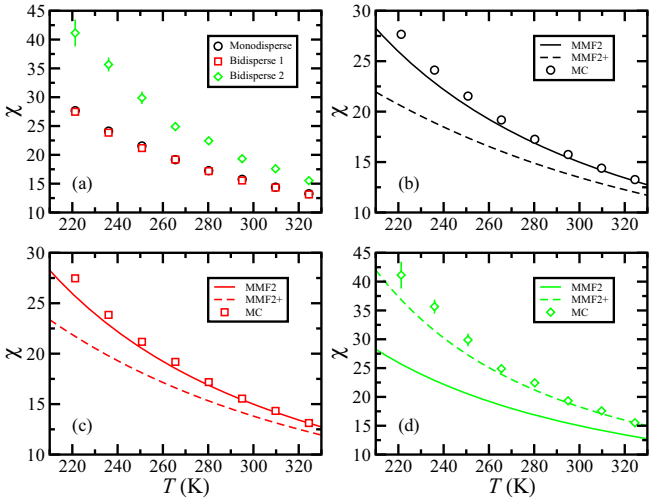

FIG. 10. Initial susceptibility as a function of temperature for monodisperse and polydisperse ferrofluids with $M(\infty) = 75\,\mathrm{kA\,m^{-1}}$: (a) all simulation results; (b) monodisperse configuration; (c) bidisperse configuration 1; and (d) bidisperse configuration 2. The points are from MC simulations, the solid lines are from MMF2 theory, and the dashed lines are from MMF2+ theory.

configuration and bidisperse configuration 1, and that MMF2+ works best for bidisperse configuration 2.

Figure 10 shows the initial susceptibility over the temperature range $221.25 \leqslant T \leqslant 324.50$ K. The direct comparison of simulation results [panel (a)] shows that bidisperse configuration 2 consistently has a much higher susceptibility than the other two configurations, which are very similar to one another over the whole temperature range. The comparisons with theory [panels (b)–(d)] show that MMF2 is best for the monodisperse configuration and bidisperse configuration 1, and that MMF2+ is accurate for bidisperse configuration 2.

These results are consistent with those presented in Sec. III A. When the ferrofluid has low polydispersity, and therefore does not contain particles large enough to form aggregates, then the MMF2 theory is most accurate; this is the case for the monodisperse configuration and bidisperse configuration 1. When the ferrofluid has high polydispersity, and does contain aggregated large particles, then the MMF2+ theory is most accurate; this is the case for the polydisperse configuration and bidisperse configuration 2.

The relationship between the initial susceptibilities of the monodisperse and bidisperse configurations is shown as the ratio $\chi_{\mathrm{bidi}}/\chi_{\mathrm{mono}}$ in Fig. 4(b). Here the simulation results are compared to both the pure-MMF2+ prediction and the ratio of the MMF2+ and MMF2 predictions for the bidisperse and monodisperse configurations, respectively. The MMF2+ theory predicts that $\chi_{\mathrm{bidi}}/\chi_{\mathrm{mono}} > 1$ for both configurations, which is true for bidisperse configuration 2, but for bidisperse configuration 1 the ratio is almost equal to 1, as would be expected if χ depended only on χ_{L}. The mixed MMF2+/MMF2 curve for bidisperse configuration 2 agrees well with the simulation results, but the agreement for bidisperse configuration 1 is not as good. Clearly neither approach gets the precise behavior correct for both configurations.

IV. CONCLUSIONS

A MMF theory of the magnetic properties of concentrated, high-susceptibility ferrofluids has been completed by derivation of the magnetization curve to supplement the known expression for the initial susceptibility. The basic approach is to determine the effective field felt by a particle due to the external magnetic field and the orientational correlations induced in all of the other particles, and then the magnetization curve is given by the familiar Langevin expression but with the effective field in place of the external magnetic field. The accuracy of the new MMF2+ theory is controlled by an expansion of the pair correlation function, and the final expression for χ contains all terms up to $\rho^3\lambda^4$. The widely used MMF2 theory only contains terms of order χ_{L}, χ_{L}^2, and χ_{L}^3, where $\chi_{\mathrm{L}} \propto \rho\lambda$. All of the results are generalized to take account of particle-size polydispersity, something that is not always given the attention it deserves [31].

Both theories have been tested against simulation results for systems with well-defined particle-size distributions, equal saturation magnetizations, the same Langevin susceptibilities, and over a broad range of temperature. It is found that the MMF2 and MMF2+ theories work best for moderately concentrated monodisperse and polydisperse systems, respectively. Neither theory is very accurate for the polydisperse ferrofluid at low concentration, although the MMF2+ theory performs much better than the MMF2 theory. This was shown to be due to the presence of large-particle aggregates stabilized by strong dipole-dipole interactions, which require extra terms in the expansions of the effective field and the initial susceptibility. At high concentration, neither theory works very well, and this appears to be due to the strong structuring arising from the short-range repulsions.

The idea that large-particle correlations require extra terms in powers of λ was confirmed by studying two moderately concentrated bidisperse ferrofluids with the same saturation magnetization and Langevin susceptibility: one contained large particles that were not large enough to aggregate, and in this case the MMF2 theory worked best; the other contained large particles that can aggregate, and in this case the MMF2+ theory worked best. Therefore, the MMF2+ theory captures some of the effects of large-particle aggregation in polydisperse ferrofluids, but as noted in Sec. I, including extra terms in λ is not guaranteed to give successively better results in the strong-interaction regime. This also applies to monodisperse ferrofluids with strong dipolar interactions; from the present work, it would appear that $\lambda \simeq 2$ is moderately large.

The technical reasons for this behavior lie in the values of Λ_0, Λ_1, and Λ_2 in Eq. (29). For highly polydisperse ferrofluids, Λ_0 becomes very large, and it needs the small-and-positive Λ_1 term and the large-and-negative Λ_2 term for counterbalance, mainly the latter. Therefore, ferrofluids with a large-particle component are best described with the MMF2+ theory. For monodisperse ferrofluids, and ferrofluids without a large-particle component, the Λ_1 and Λ_2 terms tip the balance the other way, and they lead to an underestimate of the susceptibility, as noted in Sec. II B.

This work provides generally quite reliable theoretical expressions for fitting the magnetic properties of concentrated

ferrofluids down to low temperatures, and with high magnetic susceptibilities up to $\chi \sim 100$. Highly concentrated ferrofluids still represent a challenge due to the need to capture both the dipolar correlations and the short-range correlations in the same theoretical framework, but for systems of moderate concentration (here meaning $\varphi \lesssim 0.38$) the MMF2+ theory appears to be reliable.

ACKNOWLEDGMENTS

E.A.E. and A.O.I. gratefully acknowledge research funding from the Ministry of Education and Science of the Russian Federation (Contract No. 02.A03.21.0006 and Project No. 3.1438.2017/4.6). The work of A.Yu.S. was supported by the Russian Foundation for Basic Research (Project No. 16-31-00089 mol_a).

APPENDIX A: EXPANSION OF $g(1,2)$

Differentiation of Eq. (22) with $n = 2$ brings down factors of U_d and U_d^2 into the integrand. The key step in the expansion of $g(1,2)$ is to separate out the terms in U_d and U_d^2 that depend on the coordinates of particles 1 and/or 2. The dipolar energy itself is easy enough:

$$U_\mathrm{d} = u_\mathrm{d}(1,2) + (N-2)u_\mathrm{d}(1,3) + (N-2)u_\mathrm{d}(2,3) + \tfrac{1}{2}(N-2)(N-3)u_\mathrm{d}(3,4). \tag{A1}$$

U_d^2 is much more complicated, but the end result is

$$\begin{aligned} U_\mathrm{d}^2 = {} & u_\mathrm{d}^2(1,2) + (N-2)u_\mathrm{d}^2(1,3) + (N-2)u_\mathrm{d}^2(2,3) + \tfrac{1}{2}(N-2)(N-3)u_\mathrm{d}^2(3,4) \\ & + 2(N-2)[u_\mathrm{d}(1,2)u_\mathrm{d}(1,3) + u_\mathrm{d}(1,2)u_\mathrm{d}(2,3) + u_\mathrm{d}(1,3)u_\mathrm{d}(2,3)] \\ & + (N-2)(N-3)[u_\mathrm{d}(1,3)u_\mathrm{d}(1,4) + u_\mathrm{d}(2,3)u_\mathrm{d}(2,4)] \\ & + 2(N-2)(N-3)[u_\mathrm{d}(1,3)u_\mathrm{d}(3,4) + u_\mathrm{d}(2,3)u_\mathrm{d}(3,4)] \\ & + (N-2)(N-3)(N-4)u_\mathrm{d}(3,4)u_\mathrm{d}(4,5) \\ & + (N-2)(N-3)u_\mathrm{d}(1,2)u_\mathrm{d}(3,4) + 2(N-2)(N-3)u_\mathrm{d}(1,3)u_\mathrm{d}(2,4) \\ & + (N-2)(N-3)(N-4)[u_\mathrm{d}(1,3)u_\mathrm{d}(4,5) + u_\mathrm{d}(2,3)u_\mathrm{d}(4,5)] \\ & + \tfrac{1}{4}(N-2)(N-3)(N-4)(N-5)u_\mathrm{d}(3,4)u_\mathrm{d}(5,6). \end{aligned} \tag{A2}$$

One can check that the total number of terms is $[N(N-1)/2]^2$, as it should be. With these expressions, it is straightforward but tedious to determine the derivatives of $g(1,2)$, using the definition of the n-particle distribution function in Eq. (22). The first derivative is [24]

$$\begin{aligned} \left[\frac{\partial g(1,2)}{\partial \epsilon}\right]_{\epsilon=0} = {} & -g_\mathrm{s}(1,2)\beta u_\mathrm{d}(1,2) - \rho \int d3\, g_\mathrm{s}(1,2,3)[\beta u_\mathrm{d}(1,3) + \beta u_\mathrm{d}(2,3)] \\ & - \frac{1}{2}\rho^2 \int d3 \int d4[g_\mathrm{s}(1,2,3,4) - g_\mathrm{s}(1,2)g_\mathrm{s}(3,4)]\beta u_\mathrm{d}(3,4). \end{aligned} \tag{A3}$$

The second derivative is much more complex,

$$\begin{aligned} \left[\frac{\partial^2 g(1,2)}{\partial \epsilon^2}\right]_{\epsilon=0} = {} & g_\mathrm{s}(1,2)[\beta u_\mathrm{d}(1,2)]^2 + \rho \int d3\, g_\mathrm{s}(1,2,3)\{[\beta u_\mathrm{d}(1,3)]^2 + [\beta u_\mathrm{d}(2,3)]^2 \\ & + 2\beta u_\mathrm{d}(1,2)\beta u_\mathrm{d}(1,3) + 2\beta u_\mathrm{d}(1,2)\beta u_\mathrm{d}(2,3) + 2\beta u_\mathrm{d}(1,3)\beta u_\mathrm{d}(2,3)\} \\ & + \frac{1}{2}\rho^2 \int d3 \int d4\, g_\mathrm{s}(1,2,3,4)\{2\beta u_\mathrm{d}(1,3)\beta u_\mathrm{d}(1,4) + 2\beta u_\mathrm{d}(2,3)\beta u_\mathrm{d}(2,4) \\ & + 4\beta u_\mathrm{d}(1,3)\beta u_\mathrm{d}(3,4) + 4\beta u_\mathrm{d}(2,3)\beta u_\mathrm{d}(3,4) + 4\beta u_\mathrm{d}(1,3)\beta u_\mathrm{d}(2,4)\} \\ & + \rho^2 \int d3 \int d4[g_\mathrm{s}(1,2,3,4) - g_\mathrm{s}(1,2)g_\mathrm{s}(3,4)]\beta u_\mathrm{d}(1,2)\beta u_\mathrm{d}(3,4) \\ & + \frac{1}{2}\rho^2 \int d3 \int d4[g_\mathrm{s}(1,2,3,4) - g_\mathrm{s}(1,2)g_\mathrm{s}(3,4)][\beta u_\mathrm{d}(3,4)]^2 \\ & + \rho^3 \int d3 \int d4 \int d5[g_\mathrm{s}(1,2,3,4,5) - g_\mathrm{s}(1,2,3)g_\mathrm{s}(4,5)] \\ & \times [\beta u_\mathrm{d}(1,3)\beta u_\mathrm{d}(4,5) + \beta u_\mathrm{d}(2,3)\beta u_\mathrm{d}(4,5)] \\ & + \rho^3 \int d3 \int d4 \int d5[g_\mathrm{s}(1,2,3,4,5) - g_\mathrm{s}(1,2)g_\mathrm{s}(3,4,5)]\beta u_\mathrm{d}(3,4)\beta u_\mathrm{d}(4,5) \\ & + \frac{1}{4}\rho^4 \int d3 \int d4 \int d5 \int d6[g_\mathrm{s}(1,2,3,4,5,6) - g_\mathrm{s}(1,2,3,4)g_\mathrm{s}(5,6) \\ & - g_\mathrm{s}(1,2)g_\mathrm{s}(3,4,5,6) - g_\mathrm{s}(1,2)g_\mathrm{s}(3,4)g_\mathrm{s}(5,6)]\beta u_\mathrm{d}(3,4)\beta u_\mathrm{d}(5,6). \end{aligned} \tag{A4}$$

At no point has the thermodynamic limit been considered; these results are exact for a finite system. It would be easy to simply truncate Eqs. (A3) and (A4) at order ρ, but there is a subtlety that should be pointed out in connection with the terms proportional to ρ^2 and which contain the difference $\Delta g_s(1,2,3,4) = g_s(1,2,3,4) - g_s(1,2)g_s(3,4)$. As discussed in Ref. [24], one must be careful in taking the thermodynamic limit, because $\Delta g_s(1,2,3,4)$ gives a term of $O(1/N)$, which will reduce the prefactor ρ^2 to ρ. To see this, it is sufficient to consider the asymptotic behavior of the distribution functions at low density, and when particles 1 and 2 are far from particles 3 and 4. The precise definition in Eq. (22), and the leading-order terms from the virial expansions of g_s [24], give

$$\Delta g_s(1,2,3,4) \approx \left(1-\frac{1}{N}\right)\left(1-\frac{2}{N}\right)\left(1-\frac{3}{N}\right)e^{-\beta u_s(1,2)-\beta u_s(3,4)} - \left(1-\frac{1}{N}\right)^2 e^{-\beta u_s(1,2)-\beta u_s(3,4)} \simeq -\frac{4}{N}e^{-\beta u_s(1,2)-\beta u_s(3,4)}. \tag{A5}$$

This means that

$$\rho^2\int d3\int d4\,\Delta g_s(1,2,3,4)[\beta u_d(3,4)]^n = -4\rho e^{-\beta u_s(1,2)}\int d\boldsymbol{\Omega}_3\int d4\,e^{-\beta u_s(3,4)}[\beta u_d(3,4)]^n, \tag{A6}$$

where the position of particle 3 has been integrated out to give a factor of V. This result can be used for each of the three relevant terms that appear in Eqs. (A3) and (A4). The final steps are to combine the expansion of $g(1,2)$ up to order ρ, insert the following approximate expressions for $g_s(1,2)$ and $g_s(1,2,3)$,

$$g_s(1,2) = [f_s(1,2)+1] + \rho[f_s(1,2)+1]\int d\boldsymbol{r}_3 f_s(1,3)f_s(2,3) + O(\rho^2), \tag{A7}$$

$$g_s(1,2,3) = [f_s(1,2)+1][f_s(1,3)+1][f_s(2,3)+1] + O(\rho), \tag{A8}$$

collect all terms that contribute to the parameter a_1, and discard everything else. The relevant terms are evaluated in Appendix B.

Note that the expansion of $g(1,2)$ can be used to calculate the Helmholtz free energy and hence all other thermodynamic functions [24]. One particularly interesting application is the determination of the phase diagram. The existence of a purely dipole-driven phase transition in monodisperse ferrofluids has long been debated: simulations suggest that there is no phase transition due to extensive chaining and ring formation [39], but that weak isotropic attractive interactions are sufficient for phase separation even in the strong-aggregation regime [40]. All standard liquid-state theories—including perturbation theories and integral equations—predict phase separation with critical temperatures at which it is known that neither significant particle aggregation nor phase separation occur; the so-called λ expansion will be no different. One interesting extension of the current approach could be to thin films of ferrofluids, in which field-induced transitions to spatially modulated hexagonal and stripe phases are known [41]; the theory could be used to evaluate the bulk contribution to the free-energy functional, expressed in terms of the nonuniform particle density.

APPENDIX B: EVALUATION OF $g(1,2)$ AND Ψ

Considering Eqs. (20), (23), (A3), (A4), (A6), (A7), and (A8), there are only five terms in $g(1,2)$ up to order ρ that contribute to a_1, and the rest are therefore irrelevant. The relevant terms are,

$$g(1,2) = \sum_{k=1}^{5} I_k + \text{irrelevant terms} + O(\rho^2). \tag{B1}$$

The five terms I_1–I_5 are as follows:

$$I_1 = f_s(1,2)+1, \tag{B2}$$

$$I_2 = \tfrac{1}{2}[f_s(1,2)+1][\beta u_d(1,2)]^2, \tag{B3}$$

$$I_3 = -\rho[f_s(1,2)+1]\left\langle\int d3[f_s(1,3)+1][f_s(2,3)+1][\beta u_d(2,3)]\right\rangle_3 = \left(\frac{\mu_0\mu_2\rho}{k_BT}\right)[f_s(1,2)+1]\left\{\frac{1}{3}(\boldsymbol{\mu}_2\cdot\boldsymbol{z})\langle\mu_3 L(\alpha_3)\rangle_3 + [3(\boldsymbol{r}_{12}\cdot\boldsymbol{\mu}_2)(\boldsymbol{r}_{12}\cdot\boldsymbol{z}) - (\boldsymbol{\mu}_2\cdot\boldsymbol{z})]\langle\mu_3 L(\alpha_3)G_1(r_{12},\sigma_1,\sigma_2,\sigma_3)\rangle_3\right\}, \tag{B4}$$

$$I_4 = \frac{1}{2}\rho[f_s(1,2)+1][\beta u_d(1,2)]^2\left\langle\int d\boldsymbol{r}_3 f_s(1,3)f_s(2,3)\right\rangle_3 = \left(\frac{\pi\rho}{24r_{12}}\right)[f_s(1,2)+1][\beta u_d(1,2)]^2\langle(\sigma_{13}+\sigma_{23}-r_{12})^2[r_{12}(r_{12}+2\sigma_{13}+2\sigma_{23})-3(\sigma_{13}-\sigma_{23})^2]\rangle_3, \tag{B5}$$

$$I_5 = \frac{1}{2}\rho[f_s(1,2)+1]\left\langle \int d3\, f_s(1,3)[f_s(2,3)+1][\beta u_d(2,3)]^2 \right\rangle_3$$
$$= \left(\frac{3\rho}{64\pi}\right)\left(\frac{\mu_0\mu_2}{k_BT}\right)^2 [f_s(1,2)+1](\boldsymbol{r}_{12}\cdot\boldsymbol{\mu}_2)^2\left\langle \mu_3^2\frac{L(\alpha_3)}{\alpha_3}G_2(r_{12},\sigma_1,\sigma_2,\sigma_3)\right\rangle_3. \quad \text{(B6)}$$

Here $\boldsymbol{z}$ is the unit vector aligned along the field direction (the laboratory z axis), and the auxiliary functions are as follows:

$$G_1(r_{12},\sigma_1,\sigma_2,\sigma_3) = \begin{cases} 0, & 0 \leqslant r_{12} < \sigma_{12}, \\ \int_{\sigma_{23}}^{r_{12}+\sigma_{13}} H_1(r_{12},r_{23},\sigma_1,\sigma_2,\sigma_3)dr_{23}, & \sigma_{12} \leqslant r_{12} < \sigma_{12}+\sigma_3, \\ \int_{r_{12}-\sigma_{13}}^{r_{12}+\sigma_{13}} H_1(r_{12},r_{23},\sigma_1,\sigma_2,\sigma_3)dr_{23}, & r_{12} \geqslant \sigma_{12}+\sigma_3, \end{cases} \quad \text{(B7)}$$

$$H_1(r_{12},r_{23},\sigma_1,\sigma_2,\sigma_3) = \frac{\left[\sigma_{13}^2-(r_{12}-r_{23})^2\right]\left[\sigma_{13}^2-(r_{12}+r_{23})^2\right]\left[\sigma_{13}^2-\left(r_{12}^2+r_{23}^2\right)\right]}{32r_{12}^3r_{23}^4}, \quad \text{(B8)}$$

$$G_2(r_{12},\sigma_1,\sigma_2,\sigma_3) = \begin{cases} 0, & 0 \leqslant r_{12} < \sigma_{12}, \\ \int_{\sigma_{23}}^{r_{12}+\sigma_{13}} H_2(r_{12},r_{23},\sigma_1,\sigma_2,\sigma_3)dr_{23}, & \sigma_{12} \leqslant r_{12} < \sigma_{12}+\sigma_3, \\ \int_{r_{12}-\sigma_{13}}^{r_{12}+\sigma_{13}} H_2(r_{12},r_{23},\sigma_1,\sigma_2,\sigma_3)dr_{23}, & r_{12} \geqslant \sigma_{12}+\sigma_3, \end{cases} \quad \text{(B9)}$$

$$H_2(r_{12},r_{23},\sigma_1,\sigma_2,\sigma_3) = \frac{\left(r_{12}^2+r_{23}^2-\sigma_{13}^2\right)^3}{4r_{12}^3r_{23}^7} - \frac{r_{12}^2+r_{23}^2-\sigma_{13}^2}{r_{12}r_{23}^5}. \quad \text{(B10)}$$

Upon substituting $g(1,2)$ into Eq. (20), five terms corresponding to I_1–I_5 will appear, such that

$$\Psi(\omega_1) = \alpha_1\cos\omega_1 + \sum_{k=1}^{5}\Psi_k(\omega_1). \quad \text{(B11)}$$

The five terms $\Psi_1(\omega_1)$–$\Psi_5(\omega_1)$ are as follows:

$$\Psi_1(\omega_1) = \frac{\rho}{3}\left(\frac{\mu_0\mu_1}{k_BT}\right)\langle\mu_2L(\alpha_2)\rangle_2\cos\omega_1 = \left(\frac{\mu_0\mu_1}{k_BT}\right)\left[\frac{1}{3}M_L(H)\right]\cos\omega_1, \quad \text{(B12)}$$

$$\Psi_2(\omega_1) = \left(\frac{\rho}{48\pi^2}\right)\left(\frac{\mu_0\mu_1}{k_BT}\right)^3\left\langle\frac{\mu_2^3}{\sigma_{12}^6}\left\{\frac{L(\alpha_2)}{25}P_1(\cos\omega_1)+\left[\frac{L_3(\alpha_2)}{105\alpha_2}-\frac{L(\alpha_2)}{525}\right]P_3(\cos\omega_1)\right\}\right\rangle_2, \quad \text{(B13)}$$

$$\Psi_3(\omega_1) = \left(\frac{\mu_0\rho}{3k_BT}\right)^2\mu_1\cos\omega_1\left\langle\mu_2^2\mu_3L(\alpha_3)\left\{L_2(\alpha_2)+\frac{(\sigma_1\sigma_2+\sigma_2\sigma_3+\sigma_1\sigma_3)^3}{160\sigma_{12}^3\sigma_{23}^3}\left[\frac{L(\alpha_2)}{\alpha_2}-2\right]\right\}\right\rangle_{2,3}$$
$$\simeq \left(\frac{\mu_0\mu_1}{k_BT}\right)\left[\frac{1}{144}M_L(H)\frac{dM_L(H)}{dH}\right]\cos\omega_1, \quad \text{(B14)}$$

$$\Psi_4(\omega_1) = \frac{71}{2880}\left(\frac{\rho^2}{4\pi\langle\sigma^3\rangle}\right)\left(\frac{\mu_0\mu_1}{k_BT}\right)^3\left\langle\mu_2^3A(\sigma_1,\sigma_2,\sigma_3)\left\{\frac{L(\alpha_2)}{25}P_1(\cos\omega_1)+\left[\frac{L_3(\alpha_2)}{105\alpha_2}-\frac{L(\alpha_2)}{525}\right]P_3(\cos\omega_1)\right\}\right\rangle_{2,3}, \quad \text{(B15)}$$

$$\Psi_5(\omega_1) = \frac{3\ln 2-7}{360}\left(\frac{\mu_0\rho}{k_BT}\right)^2\left(\frac{\mu_0\mu_1}{4\pi\langle\sigma^3k_BT\rangle}\right)\cos\omega_1\left\langle\mu_2^3\mu_3^2B(\sigma_1,\sigma_2,\sigma_3)L(\alpha_2)\frac{L(\alpha_3)}{\alpha_3}\right\rangle_{2,3}. \quad \text{(B16)}$$

The exact expression for $\Psi_3(\omega_1)$ is more complicated than the usual result from the MMF2 theory, but for all of the monodisperse and polydisperse systems studied, the numerical values coincide almost exactly, and so the simpler MMF2 result is written in Eq. (B14). In Eqs. (B12)–(B16), $L_j(z) = 1 - jL(z)/z$, and the functions A and B are given in Eqs. (26) and (27), respectively. Note that $\Psi_1(\omega_1)$, $\Psi_3(\omega_1)$, and $\Psi_5(\omega_1)$ are all proportional to $\cos\omega_1$, and so they contribute entirely to the effective Langevin parameter a_1 in Eq. (19). $\Psi_2(\omega_1)$ and $\Psi_4(\omega_1)$ each contain terms proportional to $P_1(\cos\omega_1)$ and $P_3(\cos\omega_1)$, but only the prefactors of the first Legendre polynomial $\cos\omega_1$ contribute to the effective Langevin parameter a_1. Combining Eqs. (19) and (B11) gives the effective field in Eq. (25).

In Sec. III A, the approximate expression for $g(1,2)$ given in Eq. (B1) is used to construct the zero-field radial distribution functions for small-particle, medium-particle, and large-particle fractions in a polydisperse ferrofluid, and the results are compared with simulations. In zero field, $I_3 = 0$ (B4) because it depends on $u_d(2,3)$, which disappears on orientational averaging. All of the "irrelevant terms" in Eq. (B1) are also equal to zero except one—the hard-sphere three-body term of order ρ given in Eq. (A7).

The final expression is of the form

$$g(1,2) = \left\langle \int d\mathbf{\Omega}_1 \int d\mathbf{\Omega}_2 (I_1 + I_2 + I_4 + 2I_5) + \rho[f_s(1,2) + 1] \int d\boldsymbol{r}_3 f_s(1,3) f_s(2,3) \right\rangle_{1,2}, \tag{B17}$$

where the factor of 2 in I_5 comes from topologically equivalent contributions involving $[u_d(1,3)]^2$ and $[u_d(2,3)]^2$.

[1] R. E. Rosensweig, *Ferrohydrodynamics* (Dover, New York, 1998).
[2] P. Langevin, J. Phys. Theor. Appl. **4**, 678 (1905).
[3] M. Shliomis, Usp. Fiz. Nauk **112**, 427 (1974).
[4] A. F. Pshenichnikov and A. V. Lebedev, Colloid J. **57**, 800 (1995).
[5] P. Weiss, J. Phys. Theor. Appl. **6**, 661 (1907).
[6] A. O. Tsebers, Magnetohydrodynamics **18**, 137 (1982).
[7] M. S. Wertheim, J. Chem. Phys. **55**, 4291 (1971).
[8] A. F. Pshenichnikov, A. V. Lebedev, and K. I. Morozov, Magnetohydrodynamics **23**, 31 (1987).
[9] K. I. Morozov and A. V. Lebedev, J. Magn. Magn. Mater. **85**, 51 (1990).
[10] Yu. A. Buyevich and A. O. Ivanov, Physica A **190**, 276 (1992).
[11] A. O. Ivanov and O. B. Kuznetsova, Colloid J. **63**, 60 (2001).
[12] I. Szalai, S. Nagy, and S. Dietrich, Phys. Rev. E **92**, 042314 (2015).
[13] A. F. Pshenichnikov, J. Magn. Magn. Mater. **145**, 319 (1995).
[14] A. F. Pshenichnikov, V. V. Mekhonoshin, and A. V. Lebedev, J. Magn. Magn. Mater. **161**, 94 (1996).
[15] B. Huke and M. Lücke, Phys. Rev. E **62**, 6875 (2000).
[16] B. Huke and M. Lücke, Phys. Rev. E **67**, 051403 (2003).
[17] I. Szalai and S. Dietrich, J. Phys.: Condens. Matter **20**, 204122 (2008).
[18] I. Szalai and S. Dietrich, J. Phys.: Condens. Matter **23**, 326004 (2011).
[19] I. Szalai, S. Nagy, and S. Dietrich, J. Phys.: Condens. Matter **25**, 465108 (2013).
[20] A. O. Ivanov, S. S. Kantorovich, E. N. Reznikov, C. Holm, A. F. Pshenichnikov, A. V. Lebedev, A. Chremos, and P. J. Camp, Phys. Rev. E **75**, 061405 (2007).
[21] A. O. Ivanov, S. S. Kantorovich, E. N. Reznikov, C. Holm, A. F. Pshenichnikov, A. V. Lebedev, A. Chremos, and P. J. Camp, Magnetohydrodynamics **43**, 393 (2007).
[22] A. O. Ivanov and O. B. Kuznetsova, Phys. Rev. E **64**, 041405 (2001).
[23] A. O. Ivanov and O. B. Kuznetsova, Colloid J. **68**, 430 (2006).
[24] J.-P. Hansen and I. R. McDonald, *Theory of Simple Liquids*, 2nd ed. (Academic, London, 1986).
[25] A. F. Pshenichnikov and A. V. Lebedev, J. Chem. Phys. **121**, 5455 (2004).
[26] A. F. Pshenichnikov and A. V. Lebedev, Colloid J. **67**, 189 (2005).
[27] A. V. Lebedev, Colloid J. **72**, 815 (2010).
[28] A. V. Lebedev, Colloid J. **75**, 386 (2013).
[29] A. V. Lebedev, Colloid J. **76**, 334 (2014).
[30] P. J. Camp, E. A. Elfimova, and A. O. Ivanov, J. Phys.: Condens. Matter **26**, 456002 (2014).
[31] A. O. Ivanov and E. A. Elfimova, J. Magn. Magn. Mater. **374**, 327 (2015).
[32] A. Y. Solovyova, O. A. Goldina, A. O. Ivanov, A. V. Lebedev, and E. A. Elfimova, J. Chem. Phys. **145**, 084909 (2016).
[33] M. P. Allen and D. J. Tildesley, *Computer Simulation of Liquids*, 2nd ed. (Oxford University Press, Oxford, 2016).
[34] J. J. Weis and D. Levesque, Phys. Rev. Lett. **71**, 2729 (1993).
[35] P. J. Camp and G. N. Patey, Phys. Rev. E **62**, 5403 (2000).
[36] E. A. Elfimova, A. O. Ivanov, and P. J. Camp, J. Chem. Phys. **136**, 194502 (2012).
[37] Yu. E. Nekhoroshkova, O. A. Goldina, P. J. Camp, E. A. Elfimova, and A. O. Ivanov, J. Exp. Theor. Phys. **118**, 442 (2014).
[38] A. F. Pshenichnikov, E. A. Elfimova, and A. O. Ivanov, J. Chem. Phys. **134**, 184508 (2011).
[39] L. Rovigatti, J. Russo, and F. Sciortino, Phys. Rev. Lett. **107**, 237801 (2011).
[40] G. Ganzenmüller, G. N. Patey, and P. J. Camp, Mol. Phys. **107**, 403 (2009).
[41] D. Lacoste and T. C. Lubensky, Phys. Rev. E **64**, 041506 (2001).